Journal of Materials Chemistry A

PAPER

Porosity-Engineered Carbons for Supercapacitive Energy Storage Using Conjugated Microporous Polymer Precursors

Received 00th January 20xx,
Accepted 00th January 20xx

DOI: 10.1039/x0xx00000x

www.rsc.org/

Jet-Sing M. Lee,[a] Tzu-Ho Wu,[b] Ben Alston,[a] Michael E. Briggs,[a] Tom Hasell,[a] Chi-Chang Hu[b] and Andrew I. Cooper*[a]

Conjugated microporous polymers (CMPs) are considered an important material, combining aspects of both microporosity and extended π-conjugation. However, pristine CMP electrodes suffer from poor electrical conductivity which limits the material in electrochemical applications. In this work, direct carbonisation of conjugated microporous polymers (CMPs) yields porosity-engineered carbons, important for the flow of ions through the electrode. These conductive carbonised CMPs show specific capacitance as high as 260 F g^{-1}, excellent rate capability and no loss in performance after 10000 charge/discharge cycles. This study provides a procedure to enhance the performance of CMP-based materials, opening up a new source of electroactive materials.

Introduction

Supercapacitors are energy-storage devices characterised by high-power density, long cycle life, and rapid charge/discharge capability.[1] The demand for new supercapacitive materials is driven by technological advances in electronic devices and in transportation requiring high power and large energy density. Supercapacitive energy storage operates by electric double-layer capacitance (EDLC) or pseudocapacitance (PC) mechanisms. EDLC functions by reversible charge accumulation at the electrode-electrolyte interface. The amount of stored charge is proportional to the capacitance of the electrode,[2] thus favoring high surface area (SA) materials, although there is no linear relationship between capacitance and SA.[3, 4] By contrast, PC is Faradaic, exploiting fast reversible redox reactions at the surface of electroactive species. PC generally provides a higher energy density than EDLC, but typically at the expense of power density and cycle life.[5] One strategy for achieving high energy densities while simultaneously keeping a high power density and cycle life is to combine principles from both EDLC and PC.

In developing supercapacitive electrode materials, it is important to consider the kinetics of ion and electron transport in electrodes and at the electrode-electrolyte interface. Thus, an electrode material with fine control over pore structure and good electrical conductivity is required.[6] Activated carbons have been studied extensively but a major challenge with these materials is the poor control that exists over pore size distribution and pore structure. The process by which carbons are produced using activating agents generally results in a broad pore size distribution.[7] Templating methods have been employed to assist in the control of pore size distribution, but this still results in large pore lengths (0.5–1 μm), which make ion diffusion inefficient.

Conjugated microporous polymers (CMPs) are a class of materials that combine extended π-conjugation within a microporous framework. CMPs have emerged as useful materials for applications such as catalysis,[8-11] light harvesting,[12] carbon dioxide capture,[13, 14] superhydrophobic separations,[15] luminescence,[16] sensing,[17] and fluorescence enhancement.[18] In 2011, Kou *et al.* reported interesting specific capacitance results for an aza-CMP material.[19] However, the cyclic voltammetry (CV) profiles did not show the rectangular-like *i-E* curve traditionally observed for supercapacitors. Instead the current proportionately increased with the shift in electrode potential in both the positive and negative sweeps over the whole potential range, which can be associated with high electric resistance.[20] The resistance was predominant at faster scan rates, which is unfavorable for supercapacitor applications. Most CMPs, though conjugated in nature, are not electrically conductive due to the poor orbital overlap of the twisted benzene rings (*e.g.*, in polyarylene ethynylenes) and inefficient packing within the amorphous 3D structure. The combination of these two factors makes many if not most CMPs reported so far unsuitable for electrochemical applications. A traditional strategy to enhance conductivity in carbon-based materials is to graphitise the structure through high temperature carbonisation.[21-23] CMPs have previously been used as carbonisation precursors for gas sorption and related applications but have not yet been thoroughly investigated as a supercapacitor.[24-26]

[a] *Department of Chemistry and Centre for Materials Discovery, University of Liverpool, Crown Street, Liverpool, L69 7ZD, UK. E-mail: aicooper@liverpool.ac.uk*
[b] *Laboratory of Electrochemistry and Advanced Materials, Department of Chemical Engineering, National Tsing Hua University, Hsinchu 30013, Taiwan.*
† Electronic Supplementary Information (ESI) available. See DOI: 10.1039/x0xx00000x

In this work, we explore the effects of carbonisation on the capacitive behaviour of CMPs in aqueous electrolytes using voltammetric and galvanostatic charge-discharge techniques. We used the first reported CMP, 'CMP-1',[27] as an example to demonstrate the flexibility of this approach (Scheme 1).

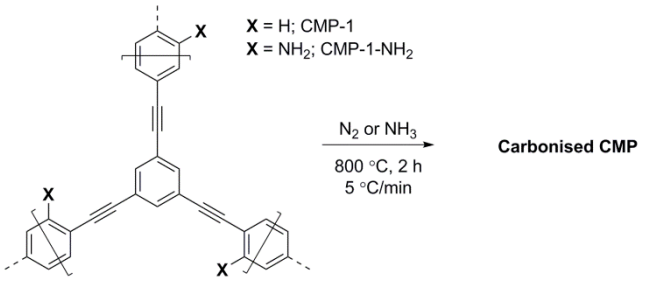

Scheme 1 Carbonisation of CMP-1.

Experimental

Preparation of CMP-1

CMP-1 was synthesised by previously reported literature methods.[27]

Preparation of CMP-1-NH_2

To a flame-dried 2-necked round bottomed flask under N_2 was added 1,3,5-triethynylbenzene (200 mg, 1.33 mmol), 2,5-dibromoaniline (334 mg, 1.33 mmol), tetrakis(triphenylphosphine)palladium(0) (61.5 mg, 4 mol%) and copper(I) iodide (20.3 mg, 8 mol%). The contents were evacuated and purged with N_2 three times and to this was added toluene (3.3 mL) and triethylamine (2 mL). The dark brown mixture was allowed to stir at 80 °C for 3 d. The resultant rusty brown mixture was allowed to cool, filtered and washed with methanol. The product was further purified by Soxhlet extraction with methanol overnight. The contents were then dried in a vacuum oven at 80 °C overnight to yield a light brown powder (93 % yield).

Preparation of C1-CMP-1

CMP (300 mg) was homogeneously dispersed into a ceramic boat. The ceramic boat was then put into a tube furnace. The sample was exposed to a flow of N_2 at room temperature for 30 min and then heated to 800 °C with a heating rate of 5 °C min^{-1} for 2 h and then cooled down to room temperature. The resultant black powder was used as obtained.

Preparation of C2-CMP-1

This follows the preparation of C1-CMP-1 but was held at set point for 6 h.

Preparation of N1-CMP-1

This follows the preparation of C1-CMP-1 but CMP-1-NH_2 was used as a precursor.

Preparation of N2-CMP-1

This follows the preparation of C1-CMP-1 but ammonia gas was initially used until heating at set point for 2 h was complete then the gas flow was switched with a N_2 flow.

Preparation of N3-CMP-1

This follows the general preparation of N2-CMP-1 but C1-CMP-1 was used as the precursor.

Preparation of electrodes

Graphite substrates (10 x 10 x 5 mm, Well Hand Industrial Corp.) were polished using fine sand paper and sonicated with deionised water in an ultrasonic bath for 10 min, then with 0.5 M H_2SO_4 for 10 min and finally with deionised water for 30 min. The substrates were then dried in an oven at 80 ˚C overnight. The mass of the electrodes were then measured. Active material (8 mg, 80 wt%) was mixed with Super C65 carbon black (1 mg, 10 wt%) and poly(vinylidine difluoride) (PVDF, 1 mg, 10 wt%, Timical) in *N*-methylpyrrolidinone (NMP, 1 mL) solvent. The resulting slurry was homogenised by ultrasonication and a total of 1 mg of the active material mass was coated onto an exposed surface of 10 x 10 mm of the substrate by pipette. The substrate was dried at 80 ˚C overnight in an oven. Mass loading of the substrate was then weighed. The samples were weighed on a 5 decimal place balance.

Electrochemical measurements

The electrochemical responses were investigated by EC-Lab SP-200 (Bio-Logic Science Instruments SAS, France) in a three-electrode configuration. A Ag/AgCl electrode (Argenthal, 3 M KCl, 0.207 V *vs.* standard hydrogen electrode at 25 °C) was used as the reference electrode and a platinum wire was employed as the counter electrode. A Luggin capillary was used to minimize errors due to ohmic potential (*iR*) drop in the electrolyte. Electrolyte solution was degassed for at least 30 min with N_2. The electrolytes for evaluating the capacitive performances were 1 M H_2SO_4, 1 M Na_2SO_4 and 3 M KOH. The specific capacitance (C_s) from CV was calculated using the following equation: $C_s = (q_a + q_c)/(2ms\Delta V)$,[28-30] where q_a and q_c represents the anodic and cathodic charge integrated from the positive and negative sweeps of the CV, m is the mass loading of active material, s is the potential scan speed and ΔV corresponds to the potential window of the CV. The specific capacitance from charge-discharge profiles was calculated using the following equation: $Cs = (I \times t)/(V \times m)$,[30] where I is the discharge current, t is discharge time, V is the discharge voltage and m is the mass of active material on the electrode.

Results and Discussion

Using a heating ramp rate of 5 °C min^{-1}, CMP-1 was carbonised at 800 °C for 2 h or 6 h under a N_2 atmosphere. The resulting carbons, without post-treatment were labelled

Table 1 Pore characteristics of the pre-and post-carbonised CMPs.

Sample	Surface area/m^2 g^{-1} BET method	Surface area/m^2 g^{-1} Langmuir method	Total pore volume[a] /cm^3 g^{-1}	Pore volume /cm^3 g^{-1} Micro-pore[b]	Pore volume /cm^3 g^{-1} Total pore[c]
CMP-1	692	873	0.41	0.18	0.36
CMP-1-NH_2	522	500	1.07	0.04	0.53
C1-CMP-1	608	633	0.33	0.22	0.32
C2-CMP-1[d]	577	601	0.31	0.21	0.28
N1-CMP-1	791	807	1.15	0.18	0.84
N2-CMP-1[e]	1139	1158	0.64	0.40	0.58
N3-CMP-1[e]	1436	1451	0.76	0.51	0.71

[a] At P/P_0 = 0.99. [b] Determined by t-plot method. [c] Determined by DFT method. [d] Held at set-point for 6 h. [e] Ammonia gas was used.

C1-CMP-1 and C2-CMP-1, respectively. A set point hold time of 6 h is generally somewhat longer than for other carbonisation precursors, which typically require heating at set point of around 2 h.[31-33] This was used due to the thermally stable nature of CMP-1, which is already highly conjugated and has fewer hydrogens to remove than most other carbon precursors. The longer set point hold time for C2-CMP-1 results in a slightly more carbonised material, which can be seen by comparing the C, H, N elemental analysis (Table S1, ESI†) for C1-CMP-1 and C2-CMP-1.

N-doping is known to be beneficial for supercapacitive materials because it enables easier dipolar attraction with the electrolyte cations,[19] gives rise to additional pseudocapacitive contributions,[34] and enhances electrical conductivity.[35] An amine-functionalised CMP-1 (CMP-1-NH_2), similar to one previously synthesised in our group,[36] was carbonised in the same way as C1-CMP-1 to produce N1-CMP-1. Replacement of the N_2 gas flow with ammonia in the carbonisation process for CMP-1 allowed incorporation of additional nitrogen into the graphitised polymer, N2-CMP-1. Further carbonisation of C1-CMP-1 in the presence of ammonia afforded a third nitrogen-doped carbon, N3-CMP-1 (Table 1).

Heating of pristine or carbonised CMP-1 in the presence of ammonia resulted in a dramatic increase in porosity, concomitant with N doping, as observed by X-ray photoelectron spectroscopy (XPS). XPS of N1-CMP-1 shows a primary C 1s peak at 285 eV, a small O 1s peak at 533.3 eV, and a weak N 1s peak at 401.2 eV (Fig. 1a).[37] N2-CMP-1 and N3-CMP-1 has a dominant C 1s peak at 285 eV, a smaller signal for the O 1s peak at 533.2 eV, and a N 1s peak at 400.1 eV (Fig. 1b,c). Analysis of the C 1s peak for all the samples suggests the presence of C=C at 284.7 eV,[38] sp^2 bonded C=N at 285.5 eV and sp^3 bonded C-N at 286.9 eV.[39] These peaks verify the integration of N atoms into the carbonised CMP-1 samples (1.9 % N-C atomic ratio in N1-CMP-1; 10.4 % N-C atomic ratio in N2-CMP-1; 5.3 % N-C atomic ratio in N3-CMP-1). Further investigation of the high-resolution N 1s spectrum of these samples confirms the presence of pyridinic (398.3 ± 0.2 eV), pyrrolic (399.9 ± 0.2 eV), quaternary (401.1 ± 0.2 eV), and oxidised (402.8 ± 0.2 eV) nitrogen (Fig. 1d,e,f).[33, 37, 40] The pyridinic and pyrrolic peaks at lower binding energies contribute to the π-conjugated system with a pair of p-electrons. Substitution of carbon atoms with nitrogen in the form of "graphitic" nitrogen results in higher N 1s binding energies. The highest energy peak in this environment is commonly associated with highly electronegative oxidised nitrogen.[41] Discounting quaternary nitrogen, all other nitrogen functional groups are situated at the edges of the layers. The different methods of N-doping results in different ratios of pyridinic, pyrrolic, quaternary and oxidised nitrogen in the material, as summarised in Table S2, ESI†. The main conclusion of the nitrogen peak deconvolution analysis is that all samples contain a low amount of oxidised nitrogen although the pyridinic, pyrrolic, and quaternary functionalities are mostly present in identical quantities in N1-CMP-1, whereas pyridinic and pyrrolic nitrogen are dominant in the N2-CMP-1 and N3-CMP-1 samples, with N3-CMP-1 containing the largest amount of pyrrolic nitrogen groups.

The surface area and pore structure of each CMP precursors and carbonised CMP-1 materials were investigated by nitrogen sorption measurements at 77.3 K. Both CMP-1 and the carbonised materials produced from this precursor show predominantly Type-I isotherms, or Type I with some Type-IVa isotherm character: there is steep adsorption at low relative pressure, indicating microporosity, and a hysteresis loop around 0.5 P/P_0, indicating mesoporosity (Fig. 2a). CMP-1-NH_2 and its carbonised sample, N1-CMP-1, show Type-II isotherms with the adsorption curve increasing steeply at higher relative pressure, which can be ascribed to macroporosity. Fig. 2b shows the pore size distribution curves for these materials derived using nonlocal density functional theory (NL-DFT). After carbonisation, the pore size decreases by about 2.5 Å compared to the pristine CMP and no additional peaks are observed. This is likely due to further micropore development of the porous carbonised materials from their CMP precursors, as seen in Table 1. The result shows that it is possible to produce carbonised CMP materials with fine-tuned pore sizes that are related to the pore structure of the CMP precursor.

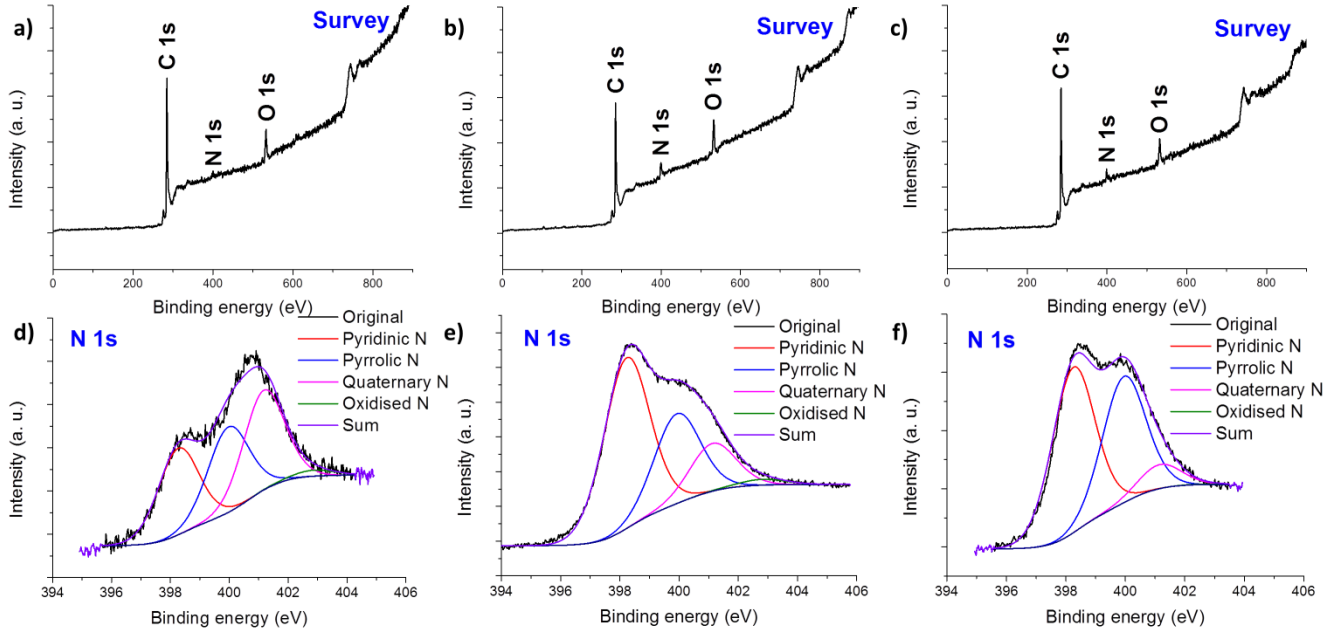

Fig. 1 XPS spectra for the (a-c) survey scans of (a) N1-CMP-1, (b) N2-CMP-1, (c) N3-CMP-1, and the (d-f) N 1s core-level spectra of (d) N1-CMP-1, (e) N2-CMP-1, (f) N3-CMP-1.

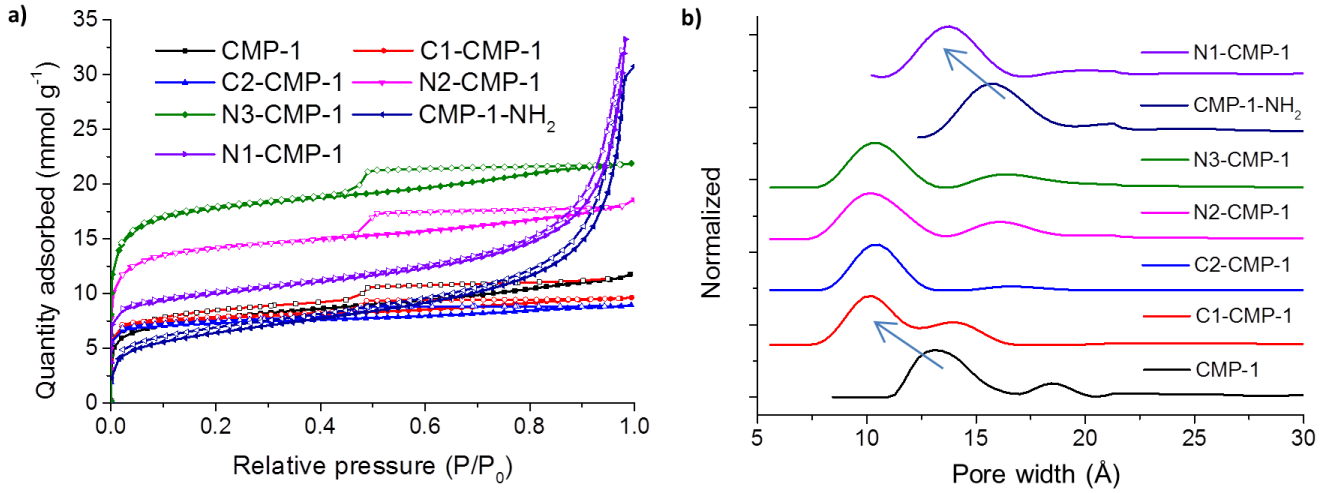

Fig. 2 (a) Nitrogen adsorption-desorption isotherms of carbonised CMPs at 77.3 K (the adsorption and desorption branches are labelled with filled and empty symbols, respectively) and (b) pore size distribution calculated by NL-DFT.

This is a significant advantage, particularly when engineering pore sizes for efficient electrolyte ion diffusion in supercapacitors, both CMP precursors seem to give better control than a previous study that uses a different porous polymer, PAF-1, as the carbon source.[42]

Field Emission Scanning Electron Microscopy (FE-SEM) was used to study the morphology of CMP-1 and the carbonised samples. The carbonised samples (Fig. S1, ESI†) all show similar morphologies to those of the parent polymer, CMP-1. This shows that the morphology of CMP-1 is retained during carbonisation, and the enhanced electrochemical properties are unlikely due to a morphology change.

Raman spectroscopy was used to investigate the graphitic structures in the carbonised CMPs (Fig. S2, ESI†). Two first-order Raman bands are present between 1100 and 1800 cm^{-1}; namely the disordered (D) band at ~1350 cm^{-1} and the graphitic (G) band at ~1590 cm^{-1} attributed to the breathing mode of *K*-point phonons of A_{1g} symmetry and the in-plane stretching motion of symmetric sp^2 C-C bonds respectively.[43, 44] Reports demonstrate that the intensity ratio I_D/I_G of the *D* and *G* bands in Raman can be used to roughly estimate the average in-plane crystallite size (L_a) of the graphene sp^2 domains (Eqn S1, ESI†).[45, 46] The I_D/I_G ratio varied from 2.29 to 2.92, which would suggest a range of crystalline domains between 31 and 40 nm within the structure. High-resolution transmission electron spectroscopy also supports some increase in ordering, with aligned features observed in the carbonised material and none in the as-made CMPs (Fig. S3, ESI†). The materials thus show evidence for enhanced long-range structure ordering after the carbonisation treatment.

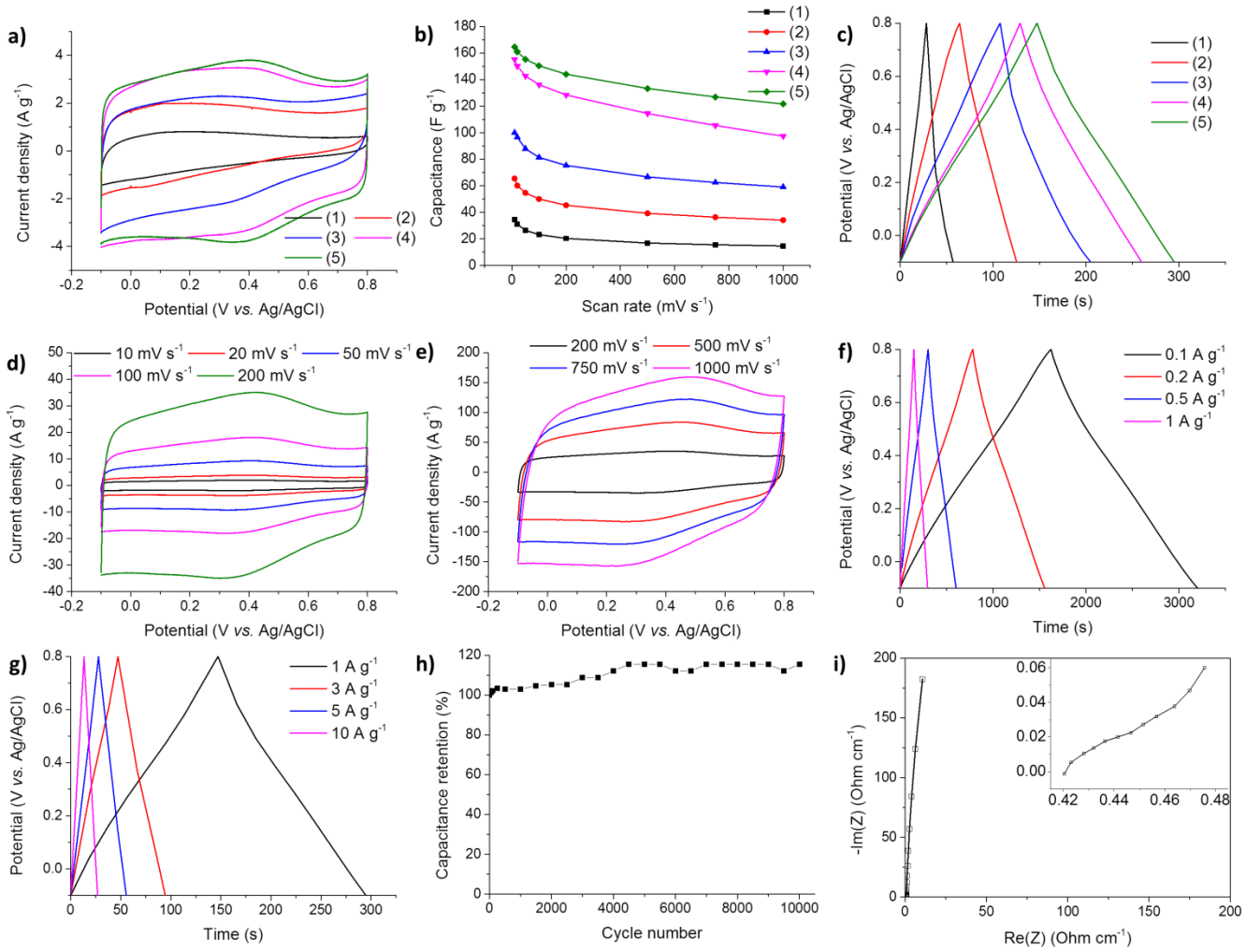

Fig. 3 (a) Cyclic voltammograms of carbonised CMPs at a scan rate of 20 mV s^{-1}: C1-CMP-1 (1), C2-CMP-1 (2), N1-CMP-1 (3), N2-CMP-1 (4) and N3-CMP-1 (5). (b) Specific capacitance at varying scan rates. (c) Galvanostatic charge-discharge curves of carbonised CMPs at a current density of 1 A g^{-1}. (d) Cyclic voltammograms of N3-CMP-1 at varying scan rates between 10 mV s^{-1} and 200 mV s^{-1}. (e) Cyclic voltammograms of N3-CMP-1 at varying scan rates between 200 mV s^{-1} and 1000 mV s^{-1}. (f) Galvanostatic charge discharge curves of N3-CMP-1 at current densities between 0.1 A g^{-1} and 1 A g^{-1}. (g) Galvanostatic charge discharge curves of N3-CMP-1 at current densities between 1 A g^{-1} and 10 A g^{-1}. (h) Cycling test of N3-CMP-1 at a current density of 5 A g^{-1}. (i) Nyquist impedance spectrum of N3-CMP-1 measured at 350 mV *vs.* Ag/AgCl in 1 M H_2SO_4.

The electrochemical performance of the resulting samples was initially evaluated by CV measurements in a 1 M H_2SO_4 aqueous electrolyte using a three-electrode cell. Fig. 3a shows the CVs of the carbonised CMP-1 samples at a scan rate of 20 mV s^{-1}. Current response was seen with C1-CMP-1 yielding a low specific capacitance of 31.0 F g^{-1} at this scan rate. This demonstrates carbonised CMP-1 has enhanced electro-chemical conductivity against its precursor. C2-CMP-1 shows an increase in current density from the CV and achieves a higher specific capacitance of 66.1 F g^{-1} at 20 mV s^{-1}. The CV curve of C2-CMP-1 also shows a more quasi-rectangular shape, which is typically characteristic of good reversible supercapacitor behaviour.[47]

Nitrogen containing carbonised CMPs showed increased performance, with capacitances of 96.5 F g^{-1} for N1-CMP-1, 150.1 F g^{-1} for N2-CMP-1, and 160.9 F g^{-1} for N3-CMP-1 at 20 mV s^{-1}. However, the CV curve of N1-CMP-1 shows a more inclined shape compared with the other samples, which may be due to limited ion diffusion.[48] This would explain why the capacitance decreases rapidly as the scan rate increases, and subsequently the transport time decreases (Fig. 3b). The ammonia-treated CMPs, N2-CMP-1 and N3-CMP-1, showed high current responses thus greater capacitive performance. The better performance of N3-CMP-1 is likely due to its higher surface area and greater volume of micropores, which contribute to the quasi-rectangular symmetrical shape that denotes a highly reversible supercapacitor. The charge-discharge times (Fig. 3c) are consistent with the charge densities of the CV results. All the carbonised CMP materials showed a triangular charge-discharge shape, which is typical behaviour for constant charge and discharge for supercapacitive materials. The N-doped CMPs superior function can be compared with N-doped PAF-1,[49] which showed non-triangular charge-discharge profiles. This was particularly pronounced at lower current densities, and may indicate poor reversibility, as was also indicated by the non-rectangular CV profile produced for the PAF-1 derived

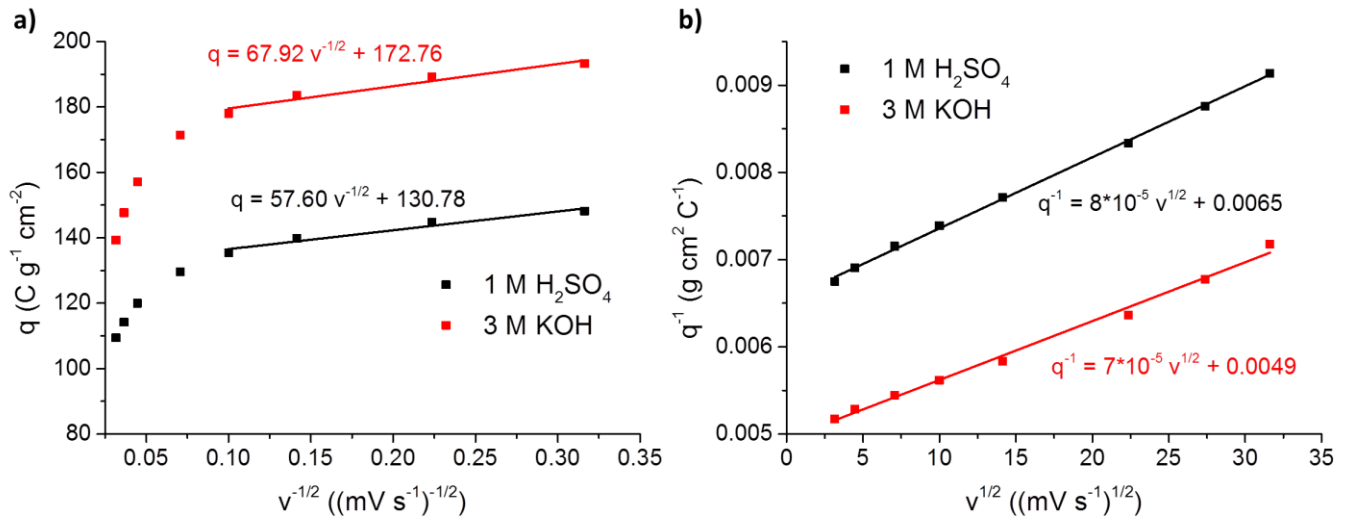

Fig. 4 (a) Dependence of q on $v^{-1/2}$ and (b) dependence of $1/q$ on $v^{1/2}$ for N3-CMP-1 in acid and basic electrolytes.

materials at faster scan speeds due to possible unideal resistance.

N3-CMP-1 shows high capacitance and possesses nearly identical voltammetric charges when integrating from both the positive and negative sweeps, indicating excellent reversibility. The electrochemical behaviour of this sample was studied further, and CV responses of N3-CMP-1 at different scan rates from 10 mV s^{-1} to 200 mV s^{-1} are shown in Fig. 3d. The CV retains a quasi-rectangular shape when the scan rate is increased, with the capacitance only reducing from 164.6 F g^{-1} at 10 mV s^{-1} to 144.0 F g^{-1} at 200 mV s^{-1}, demonstrating excellent capacitance rate-retention. Moreover, a specific capacitance of 121.6 F g^{-1} was measured at the extremely fast scan rate of 1000 mV s^{-1}. Voltammetric currents of the material also swiftly reach their respective plateau when the direction of the potential sweep is changed; even with scan rates as fast as 1000 mV s^{-1} (Fig. 3e). This indicates a low equivalent series resistance (ESR) for the material arising from its high electronic conductivity and the low ionic resistance of the electrolyte within the pores during charging and discharge.[50] The charge-discharge profile (Fig. 3f,g) also show a consistent triangular shape with varying current densities from 0.1 A g^{-1} to 10 A g^{-1}, leading to capacitances of 175.3 F g^{-1} at 0.1 A g^{-1}, 164.0 F g^{-1} at 1.0 A g^{-1}, and 148.6 F g^{-1} at 10 A g^{-1}, highlighting this material's notable capacitance retention and Coulombic efficiencies of 97 %, 100 % and 100 %, respectively. Even after 10000 charge-discharge cycles at a current density of 5 A g^{-1}, the material did not show any loss in capacitance suggesting excellent stability (Fig. 3h). In fact a slight increase in capacitance was observed which is likely due to progressive wetting of a small fraction of less accessible and therefore previously occluded pores during extended cycling. A Nyquist plot of N3-CMP-1 in the low frequency region shows the impedance of the imaginary part approaches vertical, indicative of typical ideal capacitive behaviour (Fig. 3i).[51]

The respective contributions of EDLC and PC of N3-CMP-1 can be compared against each other due to the relatively slower electrochemical kinetics that arise from Faradaic redox reactions participating in the PC mechanism,[34] originating from the same procedure in estimating the outer electroactive sites of metal oxides.[52-54] The total maximum specific capacitance, $C_{S,T,M}$, is partitioned from EDLC and PC. In this procedure, the total voltammetric charge, q_T, is calculated from estimating the charge to v = 0 from the plot of $1/q$ *vs.* $v^{1/2}$ (Fig. 4b). The specific capacitance associated with EDLC, $C_{S,DL}$, is calculated from the double-layer charge, q_{DL}, which is estimated from the charge to $v = \infty$ from the plot of q *vs.* $v^{-1/2}$ (Fig. 4a). The PC charge can be obtained by the difference between q_T and q_{DL}. Thus, $C_{S,T,M}$, $C_{S,DL}$ and $C_{S,P}$, is calculated by dividing the corresponding charge with its respective potential window of the CV, *i.e.* 0.9 V and 1.1 V for 1 M H_2SO_4 and 3 M KOH respectively (Table 2). The presence of N-containing functional groups in the material gives rise to 14% of pseudocapacitance associated with $C_{S,T,M}$. Therefore the material possesses both EDLC and PC mechanisms which can be seen from the redox peaks in Fig. 3d.

N3-CMP-1 was also investigated using different aqueous electrolytes of varying pH. The ionic strength was kept constant to correspond to the 1 M H_2SO_4 that was used previously. Fig. 5a shows the CVs of N3-CMP-1 in 1 M Na_2SO_4 at scan speeds from 10 mV s^{-1} to 200 mV s^{-1}. The CV profile of 1 M Na_2SO_4 shows a quasi-rectangular shape with good capacitances of 116.9 F g^{-1} at 10 mV s^{-1} and 100.3 F g^{-1} at 200 mV s^{-1}. The voltammetric currents when using 1 M Na_2SO_4 aqueous electrolyte are slightly lower than when using 1 M H_2SO_4 which is a known phenomenon due to better conductivity of acidic electrolyte arising from the proton hopping mechanism in aqueous media.[55] This electrolyte also yielded symmetrical triangular charge-discharge profiles (Fig. 5b), with a specific capacitance of 145.4 F g^{-1} at 0.1 A g^{-1}. The use of 3 M KOH for N3-CMP-1 gave rise to a fair

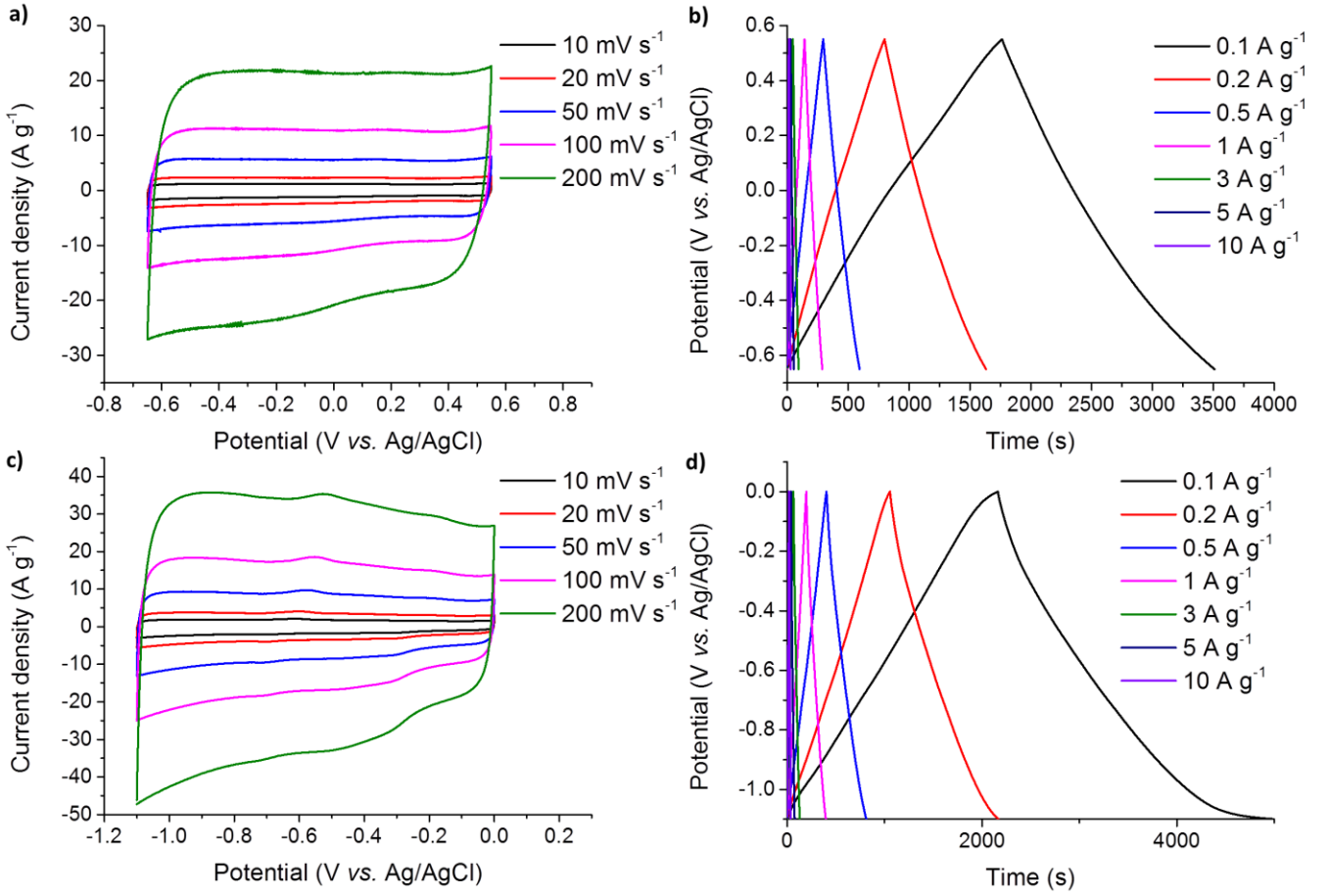

Fig. 5 (a) Cyclic voltammograms of N3-CMP-1 at varying scan rates in 1 M Na_2SO_4. (b) Galvanostatic charge-discharge curves of N3-CMP-1 at varying current densities in 1 M Na_2SO_4. (c) Cyclic voltammograms of N3-CMP-1 at varying scan rates in 3 M KOH. (d) Galvanostatic charge-discharge curves of N3-CMP-1 at varying current densities in 3 M KOH.

Table 2 Summary of maximum total specific capacitance ($C_{S,T,M}$), double-layer capacitance ($C_{S,DL}$) and pseudocapacitance ($C_{S,P}$) of N3-CMP-1 in acidic and basic electrolyte.

Electrolyte	$C_{S,T,M}$ (F g^{-1})	C_{DL} (F g^{-1})	C_P (F g^{-1})	$C_P/C_{S,T,M}$ (%)
1 M H_2SO_4	169.5	145.3	24.2	14.3
3 M KOH	185.2	157.1	28.1	15.2

quasi-rectangular CV profile, showing capacitances of 175.7 F g^{-1} at 10 mV s^{-1}, 155.7 F g^{-1} at 200 mV s^{-1} and 127.9 F g^{-1} at 1000 mV s^{-1} (Fig. 5c). Unusually, and in contrast to the previous proton hopping argument, the specific capacitance values were higher with 3 M KOH than with 1 M H_2SO_4. The charge-discharge tests on N3-CMP-1 emphasise this showing large capacitance of 260.0 F g^{-1} at a current density of 0.1 A g^{-1} (Fig. 5d). This is not conventional for supercapacitors, although the shape of the CV was less symmetrical when using basic media, which suggests that there may be increased redox activity seen from the addition peaks. This is supported by a larger PC contribution, of 15%, towards $C_{S,T,M}$ when compared to acidic electrolyte (Table 2).

The application of carbonised CMPs to supercapacitors offers exciting opportunities, and indeed three further works on this topic were published during the preparation of this manuscript. Yuan *et al.* initially produced a pillared porous graphene framework through the Yamamoto coupling of functionalised reduced graphene oxide possessing a capacitance of 286 F g^{-1} at 10 mV s^{-1}.[56] They developed this further with a composite material composed of a CMP and graphene.[57, 58] Our results demonstrate a simpler, more direct approach that can be used for a whole library of CMPs. The approach reported by Bhosale *et al*. requires a specific N- and S- containing CMP precursor; however this yielded a non-rectangular CV profile, which suggests a more resistive material.[59]

Conclusions

In summary, conductive CMP-type materials were prepared by carbonisation of CMPs under various activation methods. Our best performing material, N3-CMP-1, shows ideal supercapacitive behaviour, with a high capacitance of 175 F g^{-1} and no signs of degradation after 10000 cycles under an acidic

electrolyte. It was also shown that more ideal capacitor behaviour can be achieved with a neutral electrolyte and that an even higher capacitance of 260 F g^{-1} can be obtained with a basic electrolyte. These promising initial results open up a new method to achieve electro-active properties from CMPs. Further optimisation of these initial findings is expected to lead to improved capacitor behaviour and storage properties.

Acknowledgements

We thank EPSRC (EP/H000925/1 and EP/N004884/1) for financial support. We thank Dr Troy Manning for assistance with the carbonisation experiments, Rob Clowes for SEM imaging, Iain Aldous for Raman spectroscopy, Dr David Hesp and Dr Vin Dhanak for XPS measurements, Dr Karl Dawson for HR-TEM measurements and Dr Bonillo Fernandez for advice.

References

1. Y. Zhu, S. Murali, M. D. Stoller, K. J. Ganesh, W. Cai, P. J. Ferreira, A. Pirkle, R. M. Wallace, K. A. Cychosz, M. Thommes, D. Su, E. A. Stach and R. S. Ruoff, *Science*, 2011, **332**, 1537-1541.
2. A. Burke, *J. Power Sources*, 2000, **91**, 37-50.
3. P. Simon and Y. Gogotsi, *Nat. Mater.*, 2008, **7**, 845-854.
4. A. G. Pandolfo and A. F. Hollenkamp, *J. Power Sources*, 2006, **157**, 11-27.
5. B. You, L. Wang, L. Yao and J. Yang, *Chem. Commun.*, 2013, **49**, 5016-5018.
6. C. Liu, F. Li, L.-P. Ma and H.-M. Cheng, *Adv. Mater.*, 2010, **22**, E28-E62.
7. J. Yan, T. Wei, W. Qiao, Z. Fan, L. Zhang, T. Li and Q. Zhao, *Electrochem. Commun.*, 2010, **12**, 1279-1282.
8. L. Chen, Y. Yang and D. Jiang, *J. Am. Chem. Soc.*, 2010, **132**, 9138-9143.
9. J.-X. Jiang, C. Wang, A. Laybourn, T. Hasell, R. Clowes, Y. Z. Khimyak, J. Xiao, S. J. Higgins, D. J. Adams and A. I. Cooper, *Angew. Chem., Int. Ed.*, 2011, **123**, 1104-1107.
10. Z. Xie, C. Wang, K. E. deKrafft and W. Lin, *J. Am. Chem. Soc.*, 2011, **133**, 2056-2059.
11. R. S. Sprick, J.-X. Jiang, B. Bonillo, S. Ren, T. Ratvijitvech, P. Guiglion, M. A. Zwijnenburg, D. J. Adams and A. I. Cooper, *J. Am. Chem. Soc.*, 2015, **137**, 3265-3270.
12. L. Chen, Y. Honsho, S. Seki and D. Jiang, *J. Am. Chem. Soc.*, 2010, **132**, 6742-6748.
13. R. Dawson, D. J. Adams and A. I. Cooper, *Chem. Sci.*, 2011, **2**, 1173-1177.
14. W. Lu, J. P. Sculley, D. Yuan, R. Krishna, Z. Wei and H.-C. Zhou, *Angew. Chem., Int. Ed.*, 2012, **51**, 7480-7484.
15. A. Li, H.-X. Sun, D.-Z. Tan, W.-J. Fan, S.-H. Wen, X.-J. Qing, G.-X. Li, S.-Y. Li and W.-Q. Deng, *Energy Environ. Sci.*, 2011, **4**, 2062-2065.
16. Y. Xu, L. Chen, Z. Guo, A. Nagai and D. Jiang, *J. Am. Chem. Soc.*, 2011, **133**, 17622-17625.
17. X. Liu, Y. Xu and D. Jiang, *J. Am. Chem. Soc.*, 2012, **134**, 8738-8741.
18. J.-X. Jiang, A. Trewin, D. J. Adams and A. I. Cooper, *Chem. Sci.*, 2011, **2**, 1777-1781.
19. Y. Kou, Y. Xu, Z. Guo and D. Jiang, *Angew. Chem., Int. Ed.*, 2011, **123**, 8912-8916.
20. C.-C. Hu and C.-C. Wang, *J. Power Sources*, 2004, **125**, 299-308.
21. I. C. Lewis, *Carbon*, 1982, **20**, 519-529.
22. L. Wang, C. Schutz, G. Salazar-Alvarez and M.-M. Titirici, *RSC Advances*, 2014, **4**, 17549-17554.
23. Y. Li, H. Zhu, F. Shen, J. Wan, X. Han, J. Dai, H. Dai and L. Hu, *Adv. Funct. Mater.*, 2014, **24**, 7366-7372.
24. B. Ashourirad, A. K. Sekizkardes, S. Altarawneh and H. M. El-Kaderi, *Chem. Mater.*, 2015, **27**, 1349-1358.
25. X. Zhuang, F. Zhang, D. Wu, N. Forler, H. Liang, M. Wagner, D. Gehrig, M. R. Hansen, F. Laquai and X. Feng, *Angew. Chem., Int. Ed.*, 2013, **52**, 9668-9672.
26. X. Zhuang, D. Gehrig, N. Forler, H. Liang, M. Wagner, M. R. Hansen, F. Laquai, F. Zhang and X. Feng, *Adv. Mater.*, 2015, **27**, 3789-3796.
27. J.-X. Jiang, F. Su, A. Trewin, C. D. Wood, N. L. Campbell, H. Niu, C. Dickinson, A. Y. Ganin, M. J. Rosseinsky, Y. Z. Khimyak and A. I. Cooper, *Angew. Chem., Int. Ed.*, 2007, **46**, 8574-8578.
28. I. L. Chen, Y.-C. Wei, T.-Y. Chen, C.-C. Hu and T.-L. Lin, *J. Power Sources*, 2014, **268**, 430-438.
29. C.-C. Hu and T.-W. Tsou, *Electrochem. Commun.*, 2002, **4**, 105-109.
30. N. L. Torad, R. R. Salunkhe, Y. Li, H. Hamoudi, M. Imura, Y. Sakka, C.-C. Hu and Y. Yamauchi, *Chem. - Eur. J.*, 2014, **20**, 7895-7900.
31. L.-M. Li, E.-H. Liu, J. Li, Y.-J. Yang, H.-J, Shen, Z.-Z. Huang, X.-X. Xiang, *Acta Phys. Chim. Sin.*, 2010, **26**, 1521-1526.
32. Z. Rozlívková, M. Trchová, M. Exnerová and J. Stejskal, *Synth. Met.*, 2011, **161**, 1122-1129.
33. L. Li, E. Liu, J. Li, Y. Yang, H. Shen, Z. Huang, X. Xiang and W. Li, *J. Power Sources*, 2010, **195**, 1516-1521.
34. Y.-H. Lee, K.-H. Chang and C.-C. Hu, *J. Power Sources*, 2013, **227**, 300-308.
35. Y. Qiu, X. Zhang and S. Yang, *PCCP*, 2011, **13**, 12554-12558.
36. R. Dawson, A. Laybourn, R. Clowes, Y. Z. Khimyak, D. J. Adams and A. I. Cooper, *Macromolecules*, 2009, **42**, 8809-8816.
37. Z.-H. Sheng, L. Shao, J.-J. Chen, W.-J. Bao, F.-B. Wang and X.-H. Xia, *ACS Nano*, 2011, **5**, 4350-4358.
38. B. You, N. Li, H. Zhu, X. Zhu and J. Yang, *ChemSusChem*, 2013, **6**, 474-480.
39. K. J. Boyd, D. Marton, S. S. Todorov, A. H. Al-Bayati, J. Kulik, R. A. Zuhr and J. W. Rabalais, *J. Vac. Sci. Technol. A*, 1995, **13**, 2110-2122.
40. T. Fuller, C. Hartnig, V. Ramani, H. Uchida, H. A. Gasteiger, S. Cleghorn, P. Strasser, T. Zawodzinski, D. Jones, P. Shirvanian, T. Jarvi, P. Zelenay and P. B. C. Lamy, *Proton Exchange Membrane Fuel Cells 9*, Vienna, Austria, 2009.
41. F. Xu, M. Minniti, P. Barone, A. Sindona, A. Bonanno and A. Oliva, *Carbon*, 2008, **46**, 1489-1496.
42. Y. Li, S. Roy, T. Ben, S. Xu and S. Qiu, *PCCP*, 2014, **16**, 12909-12917.
43. N. J. Bell, Y. H. Ng, A. Du, H. Coster, S. C. Smith and R. Amal, *J. Phys. Chem. C*, 2011, **115**, 6004-6009.
44. D. Mhamane, W. Ramadan, M. Fawzy, A. Rana, M. Dubey, C. Rode, B. Lefez, B. Hannoyer and S. Ogale, *Green Chemistry*, 2011, **13**, 1990-1996.
45. F. Tuinstra and J. L. Koenig, *J. Chem. Phys.*, 1970, **53**, 1126-1130.

46. L. G. Cançado, K. Takai, T. Enoki, M. Endo, Y. A. Kim, H. Mizusaki, A. Jorio, L. N. Coelho, R. Magalhães-Paniago and M. A. Pimenta, *Appl. Phys. Lett.*, 2006, **88**, 163106.
47. E. Raymundo-Piñero, M. Cadek and F. Béguin, *Adv. Funct. Mater.*, 2009, **19**, 1032-1039.
48. J. Hu, H. Wang, Q. Gao and H. Guo, *Carbon*, 2010, **48**, 3599-3606.
49. Z. Xiang, D. Wang, Y. Xue, L. Dai, J.-F. Chen and D. Cao, *Scientific Reports*, 2015, **5**, 8307.
50. F.-C. Wu, R.-L. Tseng, C.-C. Hu and C.-C. Wang, *J. Power Sources*, 2006, **159**, 1532-1542.
51. P. L. Taberna, P. Simon and J. F. Fauvarque *J. Electrochem. Soc.*, 2003, **150**, A292-A300.
52. S. Ardizzone, G. Fregonara and S. Trasatti, *Electrochim. Acta*, 1990, **35**, 263-267.
53. D. Baronetto, N. Krstajić and S. Trasatti, *Electrochim. Acta*, 1994, **39**, 2359-2362.
54. K.-H. Chang, C.-C. Hu and C.-Y. Chou, *Chem. Mater.*, 2007, **19**, 2112-2119.
55. A. Bard and L. R. Faulkner, *Electrochemical Methods: Fundamentals and Applications*, Wiley, New York, 1980.
56. K. Yuan, Y. Xu, J. Uihlein, G. Brunklaus, L. Shi, R. Heiderhoff, M. Que, M. Forster, T. Chassé, T. Pichler, T. Riedl, Y. Chen and U. Scherf, *Adv. Mater.*, 2015, **27**, 6714-6721.
57. K. Yuan, P. Guo-Wang, T. Hu, L. Shi, R. Zeng, M. Forster, T. Pichler, Y. Chen and U. Scherf, *Chem. Mater.*, 2015, **27**, 7403-7411.
58. K. Yuan, T. Hu, Y. Xu, R. Graf, G. Brunklaus, M. Forster, Y. Chen and U. Scherf, *ChemElectroChem*, 2016, DOI: 10.1002/celc.201500516.
59. M. E. Bhosale, R. Illathvalappil, S. Kurungot and K. Krishnamoorthy, *Chem. Commun.*, 2016, **52**, 316-318.